

# Scaling of the transition temperature of hole-doped cuprate superconductors with the charge-transfer energy

C. WEBER<sup>1</sup>, C. YEE<sup>2</sup>, K. HAULE<sup>2</sup> and G. KOTLIAR<sup>2</sup>

<sup>1</sup> *T.C.M. Group - University of Cambridge, Cavendish Laboratory, J.J. Thomson Ave., Cambridge CB3 0HE, UK*

<sup>2</sup> *Department of Physics & Astronomy - Rutgers University, Piscataway, NJ 08854-8019, USA*

PACS 74.72.Gh – Hole-doped cuprate superconductors  
 PACS 74.20.Pq – Electronic structure calculations  
 PACS 74.62.-c – Transition temperature variations, phase diagrams

**Abstract** – We use first-principles calculations to extract two essential microscopic parameters, the charge-transfer energy and the inter-cell oxygen-oxygen hopping, which correlate with the maximum superconducting transition temperature  $T_{c,\max}$  across the cuprates. We explore the superconducting state in the three-band model of the copper-oxygen planes using cluster Dynamical Mean-Field Theory. We find that the variation in the charge-transfer energy largely accounts for the empirical trend in  $T_{c,\max}$ , resolving a long-standing contradiction with theoretical calculations.

arXiv:1108.3028v2 [cond-mat.str-el] 22 Oct 2012

**Introduction.** – Despite an immense body of theoretical and experimental work, we have limited microscopic insights of which materials-specific parameters govern the trends in the maximum transition temperature  $T_{c,\max}$  across the copper oxide superconductors. Structurally, all the cuprate families have in common  $\text{CuO}_2$  planes which support superconductivity. They are described by the chemical formula  $XS_{n-1}(\text{CuO}_2)_n$ , where  $n$   $\text{CuO}_2$  planes are interleaved with  $n - 1$  spacer layers  $S$  to form a multi-layer. These multi-layers are then stacked along the  $c$ -axis, separated by a different spacer layer  $X$ . Empirically, it is known that  $T_{c,\max}$  is strongly materials-dependent, ranging from 40 K in  $\text{La}_2\text{CuO}_4$  to 138 K in  $\text{HgBa}_2\text{Ca}_2\text{Cu}_3\text{O}_8$ . Additionally,  $T_{c,\max}$  can be tuned both as a function of doping and the number  $n$  of  $\text{CuO}_2$  planes.

Studies linking the known empirical trends to microscopies have generally established that the properties of the apical atoms (O, F or Cl, depending on the cuprate family) are the relevant materials-dependent parameters. However, conclusions vary regarding their effects on electronic properties, especially in multi-layer cuprates where not all  $\text{CuO}_2$  have apical atoms. Early theoretical work by Ohta, *et. al.*, found correlations between  $T_c$  and the Madelung potential of the apical oxygen, arguing that the apical potential controls the stability of the Zhang-Rice singlets [1]. They conclude that  $d_{\text{Cu-O}}^{\text{apical}}$ , the distance between the Cu and apical O, is uncorrelated with superconductivity. In a more recent DFT study, Pavarini, *et. al.*, argue that  $d_{\text{Cu-O}}^{\text{apical}}$  tunes between the single-layer cuprate

families, affecting the electronic structure primarily via the one-electron part of the Hamiltonian [2]. Moving the apical oxygens away from the copper oxide plane allows stronger coupling of in-plane O  $2p$  orbitals to the Cu  $4s$ , enhancing the strength of longer ranged hoppings. This effect is characterized by the increase of a range parameter  $r \sim t'/t$ , describing the relative strength of the next-nearest neighbor hopping  $t'$  to nearest neighbor hopping  $t$  in a one-band model. They find that materials with larger  $r$  have larger  $T_{c,\max}$ . Many-body corrections to  $t'$  were included by Yin, *et. al.* [3].

The development of cluster Dynamical Mean-Field Theory (c-DMFT) combined with first-principles calculations [4, 5] has advanced our qualitative and quantitative understanding of the cuprates [6, 7]. A satisfactory description of these materials at intermediate energy scales has been achieved, and the consensus is that the cuprates lie in the regime of intermediate correlation strength [8–10] near the Zaanen-Sawatzky-Allen (ZSA) boundary [11]. However, all numerical studies [12–14] contradict the empirical trend of  $T_{c,\max}$  with the range parameter  $r$ .

In this paper, we address the origin of the variation of the experimental  $T_{c,\max}$  across the cuprates using recent advances in electronic structure methods. We carry out first-principles calculations of the hole-doped cuprates, extract chemical parameters by downfolding to the 3-band  $p$ - $d$  model, and correlate them against  $T_{c,\max}$ . Using c-DMFT, we explore the superconducting state and identify which parameter is the key driver of transition tempera-

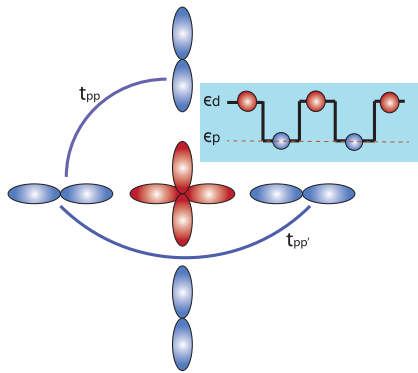


Fig. 1: Parameters of the three-band  $p$ - $d$  model for the  $\text{CuO}_2$  planes in the cuprate superconductors. We show the two shortest-ranged oxygen-oxygen hoppings  $t_{pp}$  and  $t_{pp'}$ , and the on-site energies  $\epsilon_d$  and  $\epsilon_p$ .

tures, resolving the conflict between numerics and the empirical findings of Ref. [2]. We conclude with suggestions for possible improvements in materials design to reach higher critical temperatures.

**Trends in chemical parameters.** – Effective low-energy hamiltonians containing the minimal set of bands are important tools for understanding chemical trends. We use the Wien2K code [15] to perform Linearized Augmented Plane Wave (LAPW) calculations on all major copper oxide families, and then extract model hamiltonian parameters by downfolding [16] to orbitals constructed in the manner described in Ref. [17]. In this work, we choose to downfold to a 3-band hamiltonian describing the in-plane  $\text{Cu-}3d_{x^2-y^2}$  and  $\text{O-}2p$  orbitals (Fig. 1). We believe four parameters capture the essential physics: the charge-transfer energy  $\epsilon_d - \epsilon_p$  between the Cu and O atoms, the direct Cu-O hopping  $t_{pd}$  and the two shortest-ranged O-O hoppings  $t_{pp}$ , and  $t_{pp'}$ . The extracted values are tabulated in the Supplementary Material.

We find that only two parameters,  $\epsilon_d - \epsilon_p$  and  $t_{pp'}$ , vary significantly across the cuprates. Although not crucial for our subsequent work, one would like to have a simple structural explanation for these trends. For the single-layer cuprates, the variation can be directly connected to  $d_{\text{Cu-O}}^{\text{apical}}$  (also tabulated in the Supplementary Material). As we bring the negatively-charged apical oxygen towards the CuO plane, the resulting electrostatic repulsion suppresses the hopping  $t_{pp'}$ , since  $t_{pp'}$  describes transitions of electrons past the Cu site, and provides justification for fact that  $t_{pp'}$  is smaller than  $t_{pp}$  [12]. This mechanism for the dependence of hoppings on  $d_{\text{Cu-O}}^{\text{apical}}$  has been pointed out in Ref. [2] for one-band models. However, we show in Fig. 2 that the electrostatic repulsion simultaneously increases  $\epsilon_d - \epsilon_p$  by rendering it costly to place an electron on the Cu site. These simple structural trends are less clear for multi-layer cuprates, where additional vari-

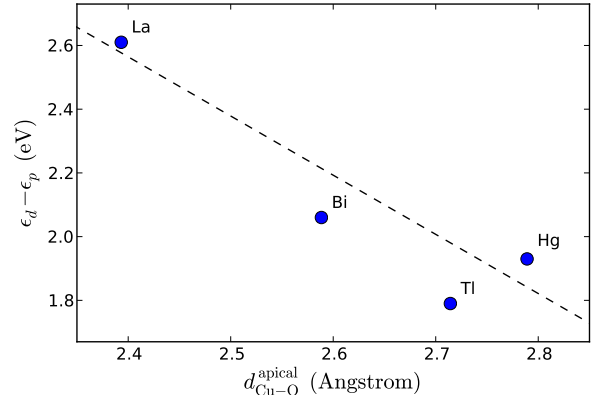


Fig. 2: In single-layer cuprates, increasing the apical oxygen distance reduces the charge-transfer energy.

ables such as the inter-layer distance introduce additional complexity.

Having identified the two relevant parameters, we plot  $T_{c,\text{max}}$  against these quantities in Fig. 3a and Fig. 3b to identify possible correlations. Beginning with  $\text{La}_2\text{CuO}_4$  (LSCO), the limiting case among the cuprates since it has the largest  $\epsilon_d - \epsilon_p$  as well as the smallest  $t_{pp'}$ , the figures show that both (i) decreasing  $\epsilon_d - \epsilon_p$  and (ii) increasing  $t_{pp'}$  correlates with an enhanced  $T_{c,\text{max}}$ . To map our results to the one-band Hubbard model, we integrate out the oxygen orbitals to extract the range-parameter  $r \sim t'/t$  (shown in Fig. 3c), and use the fact that the effective one-band correlation strength is controlled by  $\epsilon_d - \epsilon_p$  in charge-transfer materials [18]. Our results show that both the *correlation strength* and *range parameter* vary significantly across the cuprates, in contrast with Ref. [2] which focused only on the latter.

**Correlation vs. causation.** – In order to clarify how the identified microscopic parameters control  $T_{c,\text{max}}$ , we use c-DMFT in the cellular form [4, 5] with a  $2 \times 2$  cluster of impurities to solve the downfolded three-band model. The non-local self-energy in c-DMFT captures the short-ranged correlations which are crucial to describe  $d$ -wave superconductivity. Since the fermionic minus sign problem prevents impurity solvers based on quantum monte carlo from accessing the low-temperature superconducting regime, we use finite-temperature exact diagonalization (ED) at  $T = 30$  K as the impurity solver [19]. In this work, we extend previous c-DMFT calculations of the one-band model [13, 20] to the three-band model, with realistic parameters obtained from first-principles calculations. The refinement captures the admixture of the Cu and O character near the Fermi level via a bath representing both the Cu and O degrees of freedom in the DMFT self-consistency condition.

The three-band hamiltonian we treat with c-DMFT is

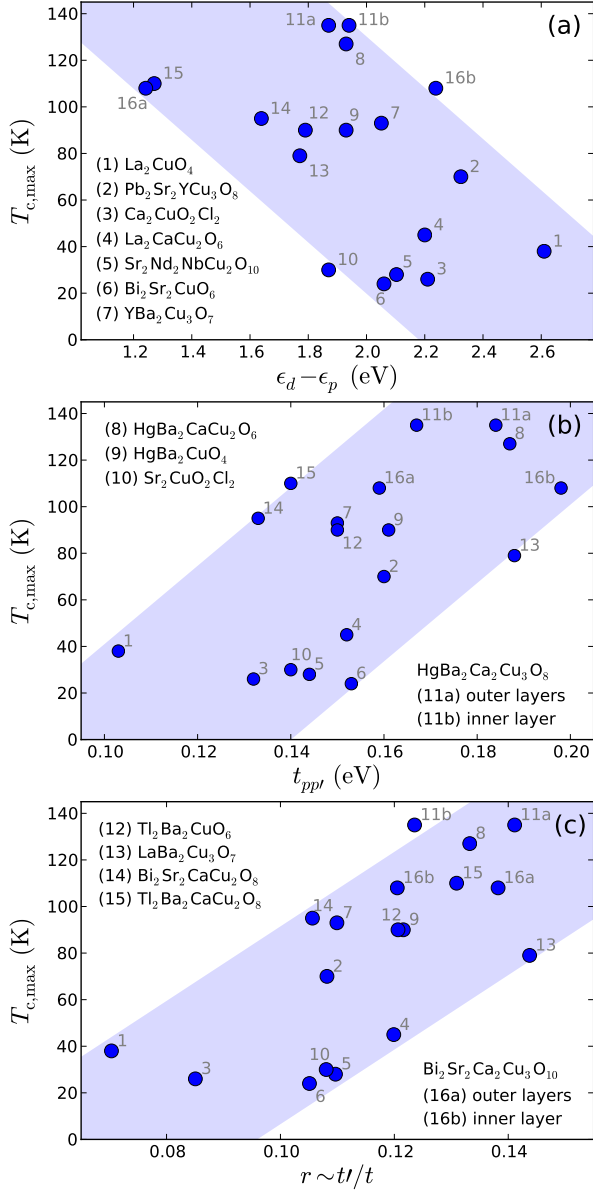


Fig. 3: Correlations of  $T_{c,\max}$  in the copper oxides with the microscopic parameters of the three-band model Hamiltonian with (a) the charge-transfer energy  $\epsilon_d - \epsilon_p$  (b) the next-nearest neighbor oxygen-oxygen hopping  $t_{pp'}$  (c) the effective one-band range parameter  $r \sim t'/t$ . The trend of the dependence of the one-band range parameter agrees with Ref. [2].

as follows:

$$H = \sum_{i\alpha j\beta\sigma} t_{ij}^{\alpha\beta} c_{i\alpha\sigma}^\dagger c_{j\beta\sigma} + \sum_{i\alpha\sigma} \epsilon_\alpha n_{i\alpha\sigma} + U_{dd} \sum_{i\sigma} n_{id\uparrow} n_{id\downarrow} \quad (1)$$

where  $i, j$  run over the in-plane  $\text{CuO}_2$  unit cells,  $\alpha, \beta$  label the orbitals  $p_x$ ,  $p_y$  and  $d_{x^2-y^2}$ , and  $\sigma$  is the electron spin. The hoppings  $t_{ij}^{\alpha\beta}$  and onsite energies  $\epsilon_\alpha$  are those sketched in Fig. 1, except for the  $d$ -orbital onsite

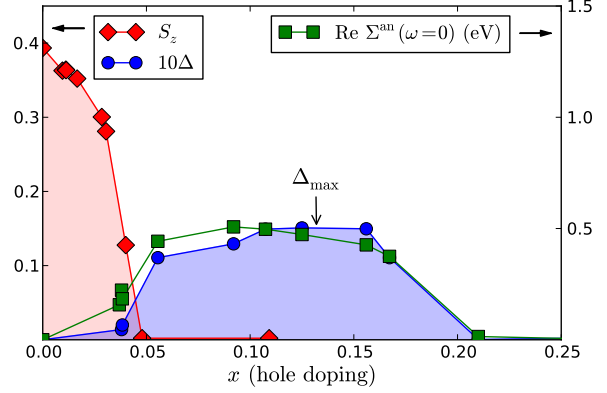


Fig. 4: Calculated doping dependence for LSCO of the staggered magnetization  $S^z = \frac{1}{2}(n_\uparrow - n_\downarrow)$  and static  $d$ -wave superconducting order parameter  $\Delta \sim \langle cc \rangle_{\tau=0}$ . We plot  $10\Delta$  to fit it on the same scale as  $S^z$ . Optimal superconducting strength  $\Delta_{\max}$  is obtained for doping  $x_{\text{opt}} \approx 0.13$ . The real part of the anomalous self-energy  $\text{Re} \Sigma^{\text{an}}(\omega=0)$  follows qualitatively the order parameter  $\Delta$ . The calculations were performed at  $T = 30$  K with c-DMFT and an ED impurity solver, using an 8-site discretization of the bath.

energy, where we subtract out a doping- and material-independent double-counting correction  $E_{\text{dc}}$  to account for correlations included in both LDA and DMFT. The atomic double-counting [21], which is very successful for all-electron DFT+DMFT [17], cannot be used because the Wannier functions of the three-band model significantly depart from the atomic wavefunctions. To determine  $E_{\text{dc}}$  for the Wannier representation, we match the low-energy Matsubara Green's function of the three-band model to the corresponding quantity in the *ab initio* all-electron calculation (see Supplementary Material). A good match was attained for  $E_{\text{dc}} = 3.12$  eV for an  $d_{x^2-y^2}$  on-site Coulomb repulsion of  $U_{dd} = 8$  eV.

To test our method, we use the extracted parameters for the canonical cuprate LSCO and explore the  $T = 0$  phase diagram as a function of doping. Our results, shown in Fig. 4, are qualitatively similar to experiment. The calculations stabilize antiferromagnetism for low dopings  $x < 0.05$ , which gives way to a dome of  $d$ -wave superconductivity. The static order parameter  $\Delta = \langle \langle c_1 c_2 \rangle \rangle_{\tau=0}$ , where 1 and 2 are nearest neighbor sites on the impurity plaquette, reaches a maximum  $\Delta_{\max}$  near  $x \sim 0.13$ . We take the magnitude of  $\Delta_{\max}$  as a proxy for the maximum superconducting temperature  $T_{c,\max}$ . The zero-frequency limit of the anomalous self-energy  $\Sigma^{\text{an}}$  is an additional indicator of superconductivity, which our results show qualitatively follows the magnitude of the order parameter.

We argue that although *two independent low-energy parameters* correlate with the experimental  $T_{c,\max}$ , it is the charge-transfer energy that controls the variation in  $\Delta_{\max}$ , and thus  $T_{c,\max}$ , across the cuprate families. To address this issue, we take the most correlated cuprate, LSCO, and compute  $\Delta_{\max}$  as we either (i) decrease  $\epsilon_d - \epsilon_p$  or (ii)

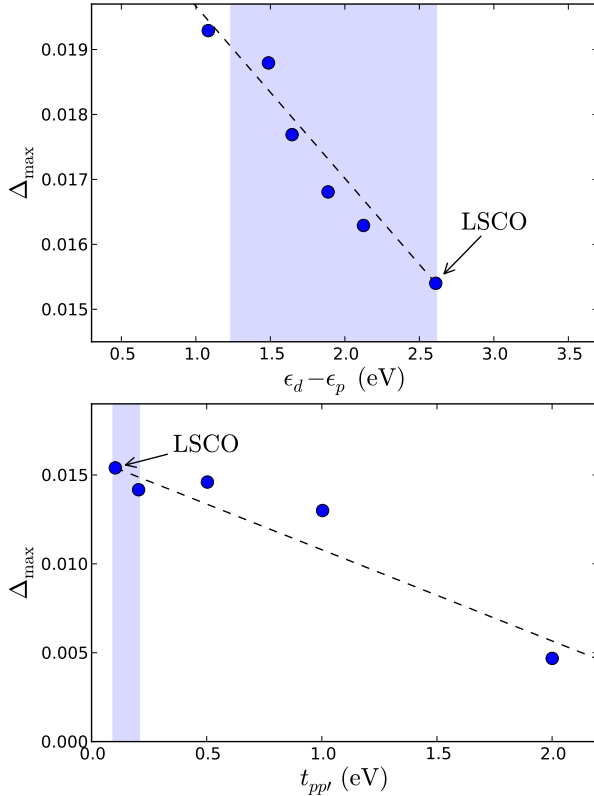


Fig. 5: Optimal superconducting order parameter  $\Delta_{\max}$  of LSCO as we (a) decrease the charge-transfer energy  $\epsilon_d - \epsilon_p$  and (b) increase oxygen-oxygen hopping  $t_{pp'}$ . Shaded are the physical ranges spanned by the cuprate families.

increase  $t_{pp'}$ . Fig. 5a shows that reducing the correlation strength for fixed  $t_{pp'}$  enhances the order parameter  $\Delta$ , in agreement with the empirical trend in Fig. 3a. However, Fig. 5b shows that increasing  $t_{pp'}$  across the physical parameter regime hardly modifies  $\Delta_{\max}$ , in contrast with the empirical trend in Fig. 3b. Further increasing  $t_{pp'}$  to larger, unphysical values strongly suppresses  $T_{c,\max}$ . Thus, our calculations support the hypothesis that a larger hopping range  $r$  suppresses  $T_{c,\max}$ , in agreement with calculations on the one-band [13,14] and three-band [12] models.

The dependence of  $T_{c,\max}$  on the two controlled parameters can be simply rationalized. For  $\epsilon_d - \epsilon_p$ , its large value in the strong correlation limit suppresses charge-fluctuations, rendering the residual superexchange interaction between the doped holes weak, resulting in low superconducting temperatures. As we decrease  $\epsilon_d - \epsilon_p$ , superconducting tendencies increase as we pass through the intermediate correlation regime, until we reach the weak correlation limit. Although the ground state of the 3-band model for large  $U_{dd}$  and  $\epsilon_d - \epsilon_p \sim 0$  has not been rigorously established, we expect the large kinetic energy to suppress the effective interactions and thus superconductivity. Thus, we believe intermediate correlation strengths, a regime intimately related to the charge-transfer metal-

to-insulator transition, is a crucial ingredient for cuprate superconductivity. Turning to  $t_{pp'}$ , we find that increasing this hopping amplitude lowers the van Hove singularity at  $(0, \pi)$  away from the Fermi level. The resulting decrease in density of states suppresses  $T_c$ , an effect which simple methods capture [22]. We note, however, that calculations based on projected BCS states find the opposite trend [23], which warrants further examination.

**Conclusions.** – We have used electronic structure methods to identify the dependence of  $T_{c,\max}$  on two fundamental parameters: the charge-transfer energy  $\epsilon_d - \epsilon_p$  and inter-cell oxygen-oxygen hopping  $t_{pp'}$ . We find that the position of the apical oxygen tunes both parameters, but the strength of superconductivity,  $\Delta_{\max}$ , is mainly sensitive to  $\epsilon_d - \epsilon_p$ . We expect future refinements to explain the remaining variability in  $T_{c,\max}$ . Our work provides a natural interpretation of experiments where epitaxial compression in LSCO resulted in an enhancement of  $T_c$  [24]. Epitaxy increases  $d_{\text{Cu-O}}^{\text{apical}}$  and thus reduces  $\epsilon_d - \epsilon_p$ . Furthermore, our result provides microscopic insight into the multi-layer cuprates, such as Bi-2223: in addition to layer-dependent doping [25], the smaller value of the charge-transfer energy in the outer layers may explain the enhancement of superconductivity in the outer layers. It has been suggested theoretically and demonstrated experimentally [26] that proximity to a metallic layer reduces the charge-transfer energy. Using this principle in heterostructure design should result in even higher transition temperatures.

\*\*\*

We thank A.-M. Tremblay and A. Millis for enlightening discussions. K.H and C.Y were supported by NSF DMR-0746395, G.K. was supported by NSF DMR-0906943, C.W. was supported by Swiss National Foundation for Science.

## REFERENCES

- [1] OHTA Y., TOHYAMA T. and MAEKAWA S., *Phys. Rev. B*, **43** (1991) 2968.
- [2] PAVARINI E., DASGUPTA I., SAHA-DASGUPTA T., JEPSEN O. and ANDERSEN O. K., *Phys. Rev. Lett.*, **87** (2001) 047003.
- [3] YIN W.-G. and KU W., *Phys. Rev. B*, **79** (2009) 214512.
- [4] KOTLIAR G., SAVRASOV S. Y., HAULE K., OUDOVENKO V. S., PARCOLLET O. and MARIANETTI C. A., *Rev. Mod. Phys.*, **78** (2006) 865.
- [5] MAIER T., JARRELL M., PRUSCHKE T. and HETTLER M. H., *Rev. Mod. Phys.*, **77** (2005) 1027.
- [6] GULL E., PARCOLLET O., WERNER P. and MILLIS A. J., *Phys. Rev. B*, **80** (2009) 245102.
- [7] HAULE K. and KOTLIAR G., *Phys. Rev. B*, **76** (2007) 104509.
- [8] COMANAC A., DE' MEDICI L., CAPONE M. and MILLIS A. J., *Nature Physics*, **4** (2008) 287.

- [9] WEBER C., HAULE K. and KOTLIAR G., *Nature Physics*, **6** (2010) 574 .
- [10] WANG X., GULL E., DE' MEDICI L., CAPONE M. and MILLIS A. J., *Phys. Rev. B*, **80** (2009) 045101.
- [11] ZAAANEN J., SAWATZKY G. A. and ALLEN J. W., *Phys. Rev. Lett.*, **55** (1985) 418.
- [12] KENT P. R. C., SAHA-DASGUPTA T., JEPSEN O., ANDERSEN O. K., MACRIDIN A., MAIER T. A., JARRELL M. and SCHULTHESS T. C., *Phys. Rev. B*, **78** (2008) 035132.
- [13] KANCHARLA S. S., KYUNG B., SÉNÉCHAL D., CIVELLI M., CAPONE M., KOTLIAR G. and TREMBLAY A.-M. S., *Phys. Rev. B*, **77** (2008) 184516.
- [14] MAIER T., JARRELL M., PRUSCHKE T. and KELLER J., *Phys. Rev. Lett.*, **85** (2000) 1524.
- [15] BLAHA P., SCHWARZ K., MADSEN G. K. H., KVASNICKA D. and LUITZ J., *WIEN2K, An Augmented Plane Wave + Local Orbitals Program for Calculating Crystal Properties* (Karlheinz Schwarz, Techn. Universität Wien, Austria) 2001.
- [16] SOUZA I., MARZARI N. and VANDERBILT D., *Phys. Rev. B*, **65** (2001) 035109.
- [17] HAULE K., YEE C.-H. and KIM K., *Phys. Rev. B*, **81** (2010) 195107.
- [18] KOTLIAR G., *Int. J. Mod. Phys. B*, **5** (1991) 341.
- [19] CAFFAREL M. and KRAUTH W., *Phys. Rev. Lett.*, **72** (1994) 1545.
- [20] CIVELLI M., *Phys. Rev. B*, **79** (2009) 195113.
- [21] ANISIMOV V. I., POTERYAEV A. I., KOROTIN M. A., ANOKHIN A. O. and KOTLIAR G., *Journal of Physics: Condensed Matter*, **9** (1997) 7359.  
<http://stacks.iop.org/0953-8984/9/i=35/a=010>
- [22] KOTLIAR G. and LIU J., *Phys. Rev. B*, **38** (1988) 5142.
- [23] PATHAK S., SHENOY V. B., RANDEKIA M. and TRIVEDI N., *Phys. Rev. Lett.*, **102** (2009) 027002.  
<http://link.aps.org/doi/10.1103/PhysRevLett.102.027002>
- [24] LOCQUET J.-P., PERRET J., FOMPEYRINE J., MCHLER E., SEO J. W. and TENDELOO G. V., *Nature*, **394** (1998) 453.
- [25] TROKINER A., LE NOC L., SCHNECK J., POUINET A. M., MELLET R., PRIMOT J., SAVARY H., GAO Y. M. and AUBRY S., *Phys. Rev. B*, **44** (1991) 2426.
- [26] ALTIERI S., TJENG L. H., VOOGT F. C., HIBMA T. and SAWATZKY G. A., *Phys. Rev. B*, **59** (1999) R2517.

# Scaling of the transition temperature of hole-doped cuprate superconductors with the charge-transfer energy

C. WEBER<sup>1</sup>, C. YEE<sup>2</sup>, K. HAULE<sup>2</sup> and G. KOTLIAR<sup>2</sup>

<sup>1</sup> *T.C.M. Group - University of Cambridge, Cavendish Laboratory, J.J. Thomson Ave., Cambridge CB3 0HE, UK*

<sup>2</sup> *Department of Physics & Astronomy - Rutgers University, Piscataway, NJ 08854-8019, USA*

PACS 74.72.Gh – Hole-doped cuprate superconductors  
 PACS 74.20.Pq – Electronic structure calculations  
 PACS 74.62.-c – Transition temperature variations, phase diagrams

**Abstract** – Supplementary material providing the details of the extraction of the materials parameters and the numerical method used to solve the 3-band Hubbard model.

arXiv:1108.3028v2 [cond-mat.str-el] 22 Oct 2012

**Appendix: Table of parameters.** – We summarize in Table 1 the parameters extracted via downfolding for the three-band model and discuss the details of the downfolding procedure.

The charge-transfer energy  $\epsilon_d - \epsilon_p$  is a localized, atomic-like quantity. Inherent in the downfolding procedure is a tradeoff between atomic character versus faithful representation low-energy bands. In order to preserve as much as possible the atomic character, we implemented the first step of the downfolding procedure described in Ref. [2]. We chose as initial orbitals  $g_n(\mathbf{r})$  the LDA+DMFT basis constructed in the manner described in Ref. [3]. The downfolding procedure is robust: we cross-checked our results by using Wien2Wannier [4] and Wannier90 [5] to perform the same downfolding procedure. Our code differs slightly in the choice of radial dependence of the trial orbitals  $g_n(\mathbf{r})$ . Again, in order to preserve the atomic character, we disabled the minimization of both spread functionals and did not use an inner window to constrain the Fermi surface. We find the extracted parameters differ by less than 5%.

In order to connect with prior work [1], we compute the range parameter  $r \sim t'/t$  using Löwdin downfolding. Beginning with the three-band model given by  $H$  equal to

$$\begin{pmatrix} \epsilon_d & 2t_{pd} \sin \frac{k_x}{2} & -2t_{pd} \sin \frac{k_y}{2} \\ 2t_{pd} \sin \frac{k_x}{2} & \epsilon_p + 2t_{pp'} \cos k_x & -4t_{pp} \sin \frac{k_x}{2} \sin \frac{k_y}{2} \\ -2t_{pd} \sin \frac{k_y}{2} & -4t_{pp} \sin \frac{k_x}{2} \sin \frac{k_y}{2} & \epsilon_p + 2t_{pp'} \cos k_y \end{pmatrix},$$

we integrate out the oxygen bands to arrive at the effective

one-band hamiltonian,

$$H_{\text{eff}}(\omega) = \epsilon_d + t_{pd} \cdot \frac{\sum_{i=0}^2 A_i(\omega) a_i(\mathbf{k})}{\sum_{i=0}^2 B_i(\omega) a_i(\mathbf{k})},$$

where we have defined the Fourier harmonics as

$$\begin{aligned} a_0(\mathbf{k}) &= 1 \\ a_1(\mathbf{k}) &= -2(\cos k_x + \cos k_y) \\ a_2(\mathbf{k}) &= 4 \cos k_x \cos k_y \end{aligned}$$

and the coefficients are

$$\begin{aligned} A_0 &= 4t_{pd}(\omega - \epsilon_p + 2t_{pp}) & B_0 &= (\omega - \epsilon_p)^2 - t_{pp}^2 \\ A_1 &= t_{pd}(\omega - \epsilon_p + 2t_{pp'} + 4t_{pp}) & B_1 &= t_{pp'}(\omega - \epsilon_p) - 2t_{pp}^2 \\ A_2 &= 2t_{pd}(t_{pp} + t_{pp'}) & B_2 &= t_{pp'}^2 - t_{pp}^2. \end{aligned}$$

Taking advantage of the fact that  $B_1/B_0$  and  $B_2/B_0$  are small, we expand out the denominator and collect coefficients of the Fourier harmonics to arrive at the range parameter

$$r \sim \frac{t'}{t} = \frac{B_0 A_2 - A_0 B_2}{B_0 A_1 - A_0 B_1} \Big|_{\omega=\epsilon_F}$$

This procedure preserves the Fermi surface and faithfully represents the low-energy band-structure. Since we prioritized the faithful representation of the atomic quantities over the non-local hopping parameters, our values of  $r \sim t'/t$  are smaller than those found in Ref. [1]. However, the trends remain unchanged.

	Compound	$\epsilon_d - \epsilon_p$	$t_{pd}$	$t_{pp}$	$t_{pp'}$	$t'/t$	layers	$d_{\text{Cu-O}}^{\text{apical}}$ (Å)	$T_c$ (K)
(1)	La <sub>2</sub> CuO <sub>4</sub>	2.61	1.39	0.640	0.103	0.070	1	2.3932	38
(2)	Pb <sub>2</sub> Sr <sub>2</sub> YCu <sub>3</sub> O <sub>8</sub>	2.32	1.30	0.673	0.160	0.108	2	2.3104	70
(3)	Ca <sub>2</sub> CuO <sub>2</sub> Cl <sub>2</sub>	2.21	1.27	0.623	0.132	0.085	1	2.7539	26
(4)	La <sub>2</sub> CaCu <sub>2</sub> O <sub>6</sub>	2.20	1.31	0.644	0.152	0.120	2	2.2402	45
(5)	Sr <sub>2</sub> Nd <sub>2</sub> NbCu <sub>2</sub> O <sub>10</sub>	2.10	1.25	0.612	0.144	0.110	2	2.0450	28
(6)	Bi <sub>2</sub> Sr <sub>2</sub> CuO <sub>6</sub>	2.06	1.36	0.677	0.153	0.105	1	2.5885	24
(7)	YBa <sub>2</sub> Cu <sub>3</sub> O <sub>7</sub>	2.05	1.28	0.673	0.150	0.110	2	2.0936	93
(8)	HgBa <sub>2</sub> CaCu <sub>2</sub> O <sub>6</sub>	1.93	1.28	0.663	0.187	0.133	2	2.8053	127
(9)	HgBa <sub>2</sub> CuO <sub>4</sub>	1.93	1.25	0.649	0.161	0.122	1	2.7891	90
(10)	Sr <sub>2</sub> CuO <sub>2</sub> Cl <sub>2</sub>	1.87	1.15	0.590	0.140	0.108	1	2.8585	30
(11a)	HgBa <sub>2</sub> Ca <sub>2</sub> Cu <sub>3</sub> O <sub>8</sub> (outer)	1.87	1.29	0.674	0.184	0.141	3	2.7477	135
(11b)	HgBa <sub>2</sub> Ca <sub>2</sub> Cu <sub>3</sub> O <sub>8</sub> (inner)	1.94	1.29	0.656	0.167	0.124	3	2.7477	135
(12)	Tl <sub>2</sub> Ba <sub>2</sub> CuO <sub>6</sub>	1.79	1.27	0.630	0.150	0.121	1	2.7143	90
(13)	LaBa <sub>2</sub> Cu <sub>3</sub> O <sub>7</sub>	1.77	1.13	0.620	0.188	0.144	2	2.2278	79
(14)	Bi <sub>2</sub> Sr <sub>2</sub> CaCu <sub>2</sub> O <sub>8</sub>	1.64	1.34	0.647	0.133	0.106	2	2.0033	95
(15)	Tl <sub>2</sub> Ba <sub>2</sub> CaCu <sub>2</sub> O <sub>8</sub>	1.27	1.29	0.638	0.140	0.131	2	2.0601	110
(16a)	Bi <sub>2</sub> Sr <sub>2</sub> Ca <sub>2</sub> Cu <sub>3</sub> O <sub>10</sub> (outer)	1.24	1.32	0.617	0.159	0.138	3	1.7721	108
(16a)	Bi <sub>2</sub> Sr <sub>2</sub> Ca <sub>2</sub> Cu <sub>3</sub> O <sub>10</sub> (inner)	2.24	1.32	0.678	0.198	0.121	3	1.7721	108

Table 1: Tight-binding parameters of the three-band  $p$ - $d$  model, containing the in-plane  $d_{x^2-y^2}$  and  $p_{(x,y)}$  orbitals, for the hole-doped cuprates (energies in eV). The table is sorted by decreasing charge-transfer energies  $\epsilon_d - \epsilon_p$ . We have included the two nearest-neighbor (intra-cell) hoppings  $t_{pd}$  and  $t_{pp}$  as well as the inter-cell oxygen-oxygen hopping  $t_{pp'}$ . Using the Löwdin procedure, we have integrated out the oxygen bands to arrive at a one-band model, from which we have extracted the ratio  $t'/t$  corresponding to the range parameter. We also include the distance between the in-plane copper and the apical atom  $d_{\text{Cu-O}}^{\text{apical}}$ . For the bilayer and trilayer compounds, we display the distance to the apical oxygens from the Cu atoms in the outer planes. The last column displays the maximum transition temperature  $T_{c,\text{max}}$  for the corresponding optimally-doped compound. See Ref. [1] and citations therein for references to experimental work on structural determination and transition temperatures of the various cuprate families.

**Appendix: Numerical method.** – To solve the three-band hamiltonian,

$$H = \sum_{i\alpha j\beta\sigma} t_{ij}^{\alpha\beta} c_{i\alpha\sigma}^\dagger c_{j\beta\sigma} + \sum_{i\alpha\sigma} \epsilon_\alpha n_{i\alpha\sigma} + U_{dd} \sum_{i\sigma} n_{id\uparrow} n_{id\downarrow} \quad (1)$$

we use in this work the realistic set of parameters shown in Table 1. We choose a  $2 \times 2$  cluster in the cellular form [6]. Cluster DMFT improves on the single site DMFT by adding a non-local self-energy. In Fig. 1.a we show the  $2 \times 2$  copper plaquette used as a unit cell through the calculations. The lattice Green's function of the four Copper site plaquette is given by:

$$\mathbf{G}_{\mathbf{k}}(i\omega_n) = (i\omega_n + \mu - \mathbf{H}_{\mathbf{k}} - \mathbf{\Sigma}(i\omega_n))^{-1}, \quad (2)$$

where  $\mathbf{H}_{\mathbf{k}}$  is the Fourier transform of the uncorrelated part of the Hamiltonian defined in Eq. 1.  $\mathbf{\Sigma}$  is the cluster self-energy matrix being nonzero only for the matrix elements connecting the  $d_{x^2-y^2}$  orbitals.

The self energy matrix in Eq. 2 is obtained by solving an  $2 \times 2$  impurity Anderson model (shown in Fig. 1b) subject to the DMFT self-consistency condition:

$$i\omega - E_{imp} - \mathbf{\Sigma}(i\omega) - \mathbf{\Delta}(i\omega) = \hat{P} \left( \sum_{\mathbf{k}} G_{\mathbf{k}}(i\omega) \right)^{-1}, \quad (3)$$

where the sum runs over the reduced Brillouin Zone (BZ), and  $\hat{P}$  is projecting the averaged green function onto the impurity cluster subspace.

In this work we use the exact diagonalization impurity solver algorithm [7]. To solve the cluster impurity problem, we express it in the form of a Hamiltonian  $H_{imp}$  with a discrete number of bath orbitals coupled to the cluster and use the Lanczos algorithm to converge the ground state of the Hamiltonian and the lower states of the spectrum. The ED method in conjunction with c-DMFT has been widely used for the one-band model [8–10].

The Anderson Impurity Model (AIM) is defined by :

$$\begin{aligned} H_{imp} = & \sum_{mn\sigma} \left( \epsilon_{mn\sigma}^n a_{m\sigma}^\dagger a_{n\sigma} + \epsilon_{mn\sigma}^a a_{m\sigma}^\dagger a_{n-\sigma}^\dagger + h.c. \right) \\ & + \sum_{mi\sigma} V_{mi\sigma} (a_{m\sigma}^\dagger c_{i\sigma} + h.c.) \\ & + \mu \sum_{i\sigma} c_{i\sigma}^\dagger c_{i\sigma} + \sum_{i\sigma} U \hat{n}_{i\uparrow} \hat{n}_{i\downarrow}. \end{aligned} \quad (4)$$

The fermionic operators  $a_{mn}^\dagger$  ( $a_{mn}$ ) creates (destroys) a particle in the bath, and the fermionic operators  $c_i^\dagger$  ( $c_i$ ) creates (destroys) a particle in the cluster of impurities. The indices  $m, n$  are running over the bath sites, and the index  $i$  is running over the impurity sites, the sites of the bath are connected by long-range hopping matrix elements through the particle-hole (particle-particle) channel  $\epsilon^n$  ( $\epsilon^a$ ), the non-correlated sites of the bath are also connected to the correlated impurities by the matrix elements  $V_{mi}$ , the onsite repulsion at the impurity sites is  $U$  (equal

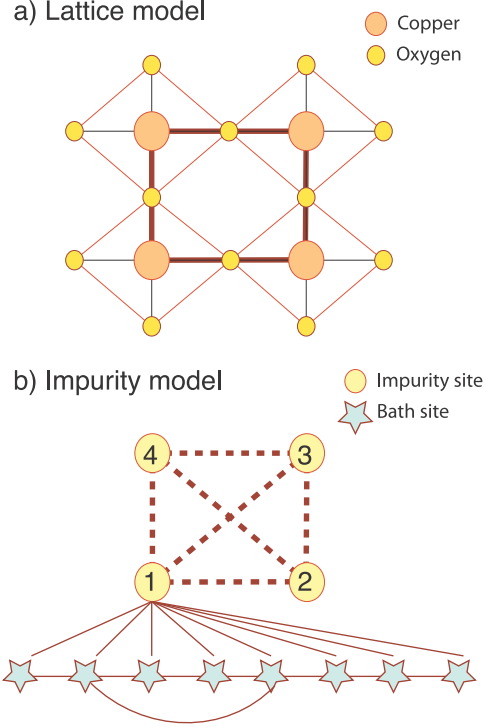


Fig. 1: (a) The d-p theoretical lattice model contains the  $p_{(x,y)}$  orbitals of the in-plane oxygen atoms (small circles) and the  $d_{x^2-y^2}$  orbital of the copper atoms (large circles). The figure shows the four copper plaquette unit-cell used in the cellular DMFT calculations. (b) The associated Anderson impurity model (AIM) contains four impurities (circles), each of them is independently connected to a bath discretized in eight sites (stars). There is not direct hybridization between the impurities, but the latter are connected by second order process through the bath (dashed lines). The sites of the bath are connected by direct and long-range hoppings.

to the Coulomb repulsion of the Copper site  $U_d$ ), and  $\mu$  is the chemical potential. We define  $\epsilon$  as the extended matrix which contains the normal  $\epsilon^n$  and anomalous  $\epsilon^a$  blocks in the Nambu basis:

$$\epsilon = \begin{pmatrix} \epsilon^n & \epsilon^a \\ (\epsilon^a)^T & -(\epsilon^n)^T \end{pmatrix} \quad (5)$$

The Weiss field  $\mathcal{G}(i\omega_n) = i\omega_n - \mathbf{\Delta}(i\omega_n) - E_{imp}$  is constructed from the parameters of the AIM:

$$\mathbf{\Delta}(i\omega_n) = \mathbf{V}^\dagger (i\omega_n - \epsilon)^{-1} \mathbf{V} \quad (6)$$

The parameters of Eq. 4 are determined by imposing the self-consistency condition in Eq. 3 using a conjugate gradient minimization algorithm:

$$d = \sum_{\omega < \omega_0, \alpha\beta} |\Delta_{\alpha\beta}^{ED}(i\omega_n) - \Delta_{\alpha\beta}(i\omega_n)|^2, \quad (7)$$

where  $\alpha\beta$  run over the matrix elements,  $\omega_0 = 20$  eV is a hard cutoff on the summation and  $\Delta^{ED}$  is a func-



tion (Eq. 6) of the Hamiltonian parameters. The fitting procedure is not exact due to the discretization of the bath and is an additional approximation to the c-DMFT scheme. In this work we considered a bath discretised with 8 energy levels. Finally, once the Hamiltonian parameters are obtained by the fitting procedure, we obtain the low energy spectrum by the Lanczos procedure. We impose an energy cutoff  $E_{max}$  such that the Boltzman weight  $e^{-\beta(E_{max}-E_0)} < 0.001$ , where  $E_0$  is the ground state energy. We discard all the eigenstates which have an energy larger than the cutoff  $E_i - E_0 > E_{max}$ . Once the eigenstates are obtained we compute the Boltzman weighted average to get the dynamical and static observables.

In this work we consider two different instabilities: i) the superconducting phase, and ii) the long-range magnetic ordered phase. The former is computed in the Nambu basis, and the Hilbert space is block diagonalized by the spin  $S^z$  quantum numbers, and the latter is obtained in the tensor product of the up and down spins. Since the number of particles is not a good quantum number in the superconducting phase, we work at fixed chemical potential. For the magnetic phase we found a better convergence when working at fixed density, with a free chemical potential.

For the determination of the phase diagram we used physical observables readily available from the  $2 \times 2$  cluster of impurities, such as the staggered magnetization  $S^z = \frac{1}{2}(n_\uparrow - n_\downarrow)$ , the superconducting order parameter  $\Delta = \langle \langle c_1 c_2 \rangle \rangle_{(\tau=0)}$  (where 1 and 2 are nearest neighbor links of the impurity plaquette) and the anomalous self-energy at zero frequency  $\Sigma^{an} \equiv \Sigma_{12}^{an}(\omega = 0)$ . We emphasize that the computed order parameters do not rely on any additional procedure, such as the  $\Sigma$ -periodization [6], which interpolates and extrapolates the discrete cluster quantities to the continuum in k-space.

Finally, we discuss the computation of the double-counting correction  $E_{dc}$ . Since the Wannier functions of the three-band  $p-d$  model is not atomic-like, we cannot use the atomic double-counting proposed in Ref. [11]. Rather, we first perform the *ab initio* all-electron calculation using the atomic double-counting,

$$E_{dc} = U \left( n_{d0} - \frac{1}{2} \right) - J \left( \frac{n_{d0}}{2} - \frac{1}{2} \right), \quad (8)$$

with  $n_{d0} = 9$ , the natural value derived from chemical valence counting. We use  $U = 10$  eV and  $J = 0.7$  eV. The atomic form of the double-counting is appropriate here because treating the full energy window causes the orbitals to be very atomic-like. In Fig. 2a, we plot the density of states from the all-electron calculation, which exhibits the charge-transfer gap of the correct magnitude (slightly less than 2 eV). Then, we select the double-counting in the  $p-d$  model so the Matsubara Green's function matches the corresponding quantity in the all-electron calculation (Fig. 2b). We find that  $E_{dc} = 3.12$  eV gives a good match, and use this value for all subsequent model calculations. Finally, we use a reduced onsite-repulsion  $U_{3\text{-band}} \approx U - 2J$

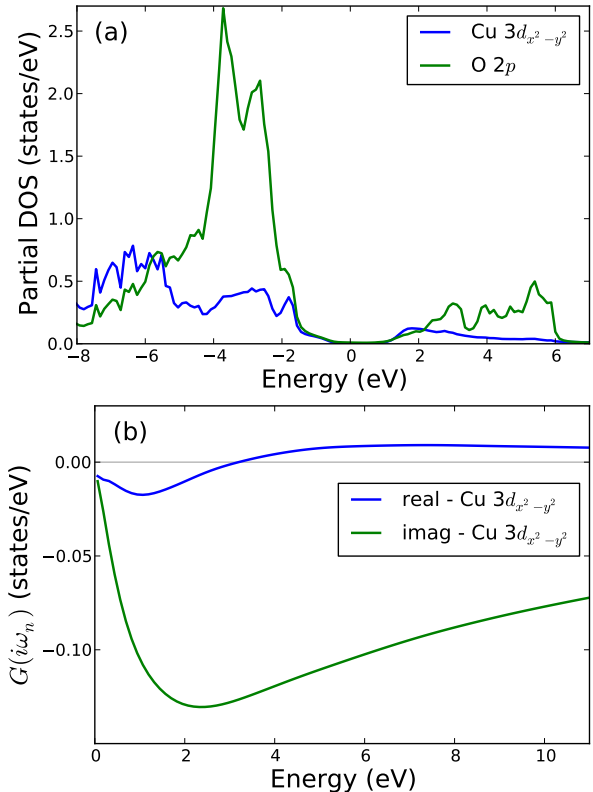


Fig. 2: (a) Density of states of LSCO from the all-electron DFT+DMFT calculation. (b) All-electron Matsubara Green's function for the Cu  $3d_{x^2-y^2}$  orbital used as reference to fix double-counting in three-band  $p-d$  model. The temperature is  $\beta = 50$  eV $^{-1}$ .

for our 3-band calculations to capture the effect of the Hund's coupling present in the all-electron calculation.

## REFERENCES

- [1] PAVARINI E., DASGUPTA I., SAHA-DASGUPTA T., JEPSEN O. and ANDERSEN O. K., *Phys. Rev. Lett.*, **87** (2001) 047003.
- [2] SOUZA I., MARZARI N. and VANDERBILT D., *Phys. Rev. B*, **65** (2001) 035109.
- [3] HAULE K., YEE C.-H. and KIM K., *Phys. Rev. B*, **81** (2010) 195107.
- [4] KUNEŠ J., ARITA R., WISSGOTT P., TOSCHI A., IKEDA H. and HELD K., *Computer Physics Communications*, **181** (2010) 1888 .
- [5] MOSTOFI A. A., YATES J. R., LEE Y.-S., SOUZA I., VANDERBILT D. and MARZARI N., *Computer Physics Communications*, **178** (2008) 685.
- [6] KOTLIAR G., SAVRASOV S. Y., PÁLSSON G. and BIROLI G., *Phys. Rev. Lett.*, **87** (2001) 186401.
- [7] CAFFAREL M. and KRAUTH W., *Phys. Rev. Lett.*, **72** (1994) 1545.
- [8] CIVELLI M., *Phys. Rev. B*, **79** (2009) 195113.

- [9] KANCHARLA S. S., KYUNG B., SÉNÉCHAL D., CIVELLI M., CAPONE M., KOTLIAR G. and TREMBLAY A.-M. S., *Phys. Rev. B*, **77** (2008) 184516.
- [10] PERRONI C. A., ISHIDA H. and LIEBSCH A., *Phys. Rev. B*, **75** (2007) 045125.
- [11] ANISIMOV V. I., POTERYAEV A. I., KOROTIN M. A., ANOKHIN A. O. and KOTLIAR G., *Journal of Physics: Condensed Matter*, **9** (1997) 7359.  
<http://stacks.iop.org/0953-8984/9/i=35/a=010>